HHS Public Access

Author manuscript

Sci Immunol. Author manuscript; available in PMC 2023 August 22.

Published in final edited form as:

Sci Immunol. 2023 July 21; 8(85): eabo4767. doi:10.1126/sciimmunol.abo4767.

NLRP11 is a pattern recognition receptor for bacterial lipopolysaccharide in the cytosol of human macrophages

Maricarmen Rojas-Lopez[1,†], **María Luisa Gil-Marqués**[1,†], **Vritti Kharbanda**[1,†], **Amanda S. Zajac**[1,†], **Kelly A. Miller**[1,†], **Thomas E. Wood**[1,†], **Austin C. Hachey**[1], **Keith T. Egger**[1], **Marcia B. Goldberg**[1,2,3,4,*]

[1]Center for Bacterial Pathogenesis, Division of Infectious Diseases, Massachusetts General Hospital, Boston, MA, USA.

[2]Department of Microbiology, Blavatnik Institute, Harvard Medical School, Boston, MA, USA.

[3]Broad Institute of MIT and Harvard, Cambridge, MA, USA.

[4]Department of Immunology and Infectious Diseases, Harvard T.H. Chan School of Public Health, Boston, MA, USA.

Abstract

Endotoxin - bacterial lipopolysaccharide (LPS) - is a driver of lethal infection sepsis through excessive activation of innate immune responses. When delivered to the cytosol of macrophages, cytosolic LPS (cLPS) induces the assembly of an inflammasome that contains caspases-4/5 in humans or caspase-11 in mice. Whereas activation of all other inflammasomes is triggered by sensing of pathogen products by a specific host cytosolic pattern recognition receptor protein,

*Corresponding author. marcia.goldberg@mgh.harvard.edu.
†These authors contributed equally to this work.

Author contributions:

M.B.G. conceptualized the project; M.R.L., M.L.G.M., V.K., A.S.Z., T.E.W., M.B.G. developed methodology used; M.R.L., M.L.G.M., V.K., A.S.Z., K.A.M., T.E.W., A.C.H., K.T.E. conducted investigation; M.L.G.M., K.A.M., A.S.Z., M.B.G. acquired funding; M.R.L., M.L.G.M., A.S.Z., K.A.M., T.E.W., M.B.G. wrote the paper.

List of Supplementary Materials:

Fig. S1. Human NLRP11 and primate homologs
Fig. S2. Generation and validation of *NLRP11* deletions
Fig. S3. *S. flexneri* infection of THP-1 macrophage-like cells lacking NLRP11
Fig. S4. Endogenous levels of innate immune proteins in *NLRP11*$^{-/-}$ macrophage-like THP-1 cells
Fig. S5. NLRP11$^{-/-}$ THP-1 macrophage-like cell response to extracellular stimulations and comparison of cLPS response with those of *CASP4*$^{-/-}$ and *GSDMD*$^{-/-}$ THP-1 macrophage-like cells
Fig. S6. Processing of caspases upon gram-negative bacterial infection or LPS electroporation of *NLRP11*$^{-/-}$ THP-1 macrophage-like cells
Fig. S7. NLRP11-dependence of release of IL-1 cytokines from THP-1 macrophage-like cells upon *S. flexneri* infection or LPS electroporation
Fig. S8. Activation of other inflammasome pathways is independent of *NLRP11*
Fig. S9. Absence of key innate immune proteins in HEK293T cells
Fig. S10. Plate binding assay of interaction of NLRP11 and caspase-4
Fig. S11. Specificity of NLRP11 interaction with caspases is independent of the tag
Fig. S12. NLRP11 role in non-canonical inflammasome activation is independent of IFNγ and induction of GBP1
Fig. S13. Recruitment of YFP-CASP4(C258S) and Myc-NLRP11 to intracellular *S. flexneri*
Table S1. Bacterial strains
Table S2. Primers for RT-PCR and RT-qPCR
Data file S1. Raw data file

Competing interests: The authors declare no competing interests.

whether pattern recognition receptors for cLPS exist has remained unclear, as caspases-4, −5, and −11 bind and activate LPS directly *in vitro*. Here, we show that the primate-specific protein NLRP11 is a pattern recognition receptor for cLPS that is required for efficient activation of the caspase-4 inflammasome in human macrophages. In human macrophages, *NLRP11* is required for efficient activation of caspase-4 during infection with intracellular gram-negative bacteria or upon electroporation of LPS. NLRP11 could bind LPS and separately caspase-4, forming a high molecular weight complex with caspase-4 in HEK293T cells. *NLRP11* is present in humans and other primates, but absent in mice, likely explaining why it has been overlooked in screens looking for innate immune signaling molecules, most of which have been carried out in mice. Our results demonstrate that NLRP11 is a component of the caspase-4 inflammasome activation pathway in human macrophages.

One Sentence Summary:

NLRP11 is a human macrophage cytosolic receptor for bacterial lipopolysaccharide.

INTRODUCTION

Inflammasomes assemble in response to the cytosolic presence of pathogen-associated molecules, including dsDNA, flagellin, type 3 secretion system structural proteins, pore-forming toxins, ion flux, ATP, and LPS (1–5). Canonical inflammasomes consist of a pattern recognition receptor, which senses a pathogen-associated molecule, and an inflammatory caspase, which are frequently linked by an adaptor protein. Inflammasome assembly activates the caspase, which proteolytically activates the pore-forming protein gasdermin D to form plasma membrane pores, leading to pyroptotic cell death (6–10). The presence of bacterial LPS in the cytosol of human macrophages activates a non-canonical inflammasome, which contains caspases-4 and −5 in humans and caspase-11 in mice (11–13), and subsequently leads to caspase-mediated processing of gasdermin D, pore formation, and pyroptotic cell death. To date, no pattern recognition receptor protein of cytosolic LPS (cLPS) has been identified, and because caspase-4, −5, and -11 bind LPS *in vitro* (14), the current paradigm is that the non-canonical inflammasome lacks a pattern recognition receptor.

Here, we identify the primate-specific nucleotide-binding oligomerization domain, leucine rich repeat and pyrin domain containing protein-11 (NLRP11) as a cytosolic pattern recognition receptor of bacterial LPS in human macrophages. We show that efficient activation of the non-canonical pathway in human-derived macrophages depends on NLRP11 and that NLRP11 interacts with core components of the caspase-4 inflammasome. Our results demonstrate that NLRP11 senses cLPS and promotes LPS-dependent activation of caspase-4.

RESULTS

NLRP11 required for cell death due to intracellular gram-negative pathogens

In a forward genetic screen conducted using a human-derived myeloid lineage cell line that enriched for genes required for death during infection with the gram-negative intracellular

bacterial pathogen *Shigella flexneri*, we identified NLRP11 as a top candidate (15) (Fig. 1A, and fig. S1). The NLRP family also includes NLRP1 and NLRP3, which sense a range of pathogen-associated molecular patterns in the cell cytosol. In human-derived monocyte THP-1 cells containing either of two targeted deletions of *NLRP11*, each homozygous for the indicated deletion (fig. S2), cell death measured by release of lactate dehydrogenase (LDH) during *S. flexneri* infection was decreased by >50% at 2h 40 min and 5h 40 min (Fig. 1B). The efficiency of cell invasion by *S. flexneri* was unaffected by the absence of NLRP11 (fig. S3A), and *S. flexneri* mutants unable to access the cytosol by virtue of inactivation of the type 3 secretion system induced minimal cell death, indicating that cell death depended on bacterial cytosolic localization and/or type 3 secretion activity (fig. S3B).

To test whether the dependence on NLRP11 for efficient cell death was generalizable to other intracellular gram-negative bacterial pathogens, we infected *NLRP11*$^{-/-}$ cells with the cytosolic pathogen *Burkholderia thailandensis* and the largely vacuolar pathogen *Salmonella enterica* serovar Typhimurium. As with *S. flexneri*, cell death during infection with *B. thailandensis* or *S.* Typhimurium was significantly reduced in *NLRP11*$^{-/-}$ macrophages (Fig. 1, C and D). Upon viral infection and certain Toll-like receptor interactions, the NF-κB pathway is repressed by NLRP11-dependent targeted degradation of TRAF6 (16–18). However, *S. flexneri*-induced NLRP11-dependent cell death was independent of TRAF6, whether or not *Shigella* OspI, which suppresses TRAF6 signaling (19), was present (fig. S3, C, D, and E), indicating that the role of NLRP11 in bacterial infection-induced cell death is distinct from its role in NF-κB signaling. The levels of CASP4, CASP1, gasdermin D, GBP1, and GBP2 were unchanged by disruption of *NLRP11* (fig. S4, A, B, and C). Levels of NLRP3 were increased in *NLRP11*$^{-/-}$ cells (fig. S4A), likely a result of TRAF6-dependent derepression of NF-κB activation of *NLRP3* expression. Levels of *CASP4* and *GSDMD* transcripts were similar in *NLRP11*$^{-/-}$ and *NLRP11*$^{+/+}$ cells, even during *S. flexneri* infection (fig S4, D and E). Moreover, tyrosine phosphorylation of STAT1 in response to IFNβ was only slightly diminished by the absence of NLRP11 (fig. S5A). Thus, NLRP11 is required for efficient cell death induced by multiple intracellular gram-negative pathogens.

NLRP11 functions in a pathway activated by cytosolic bacterial LPS

We tested whether LPS, which is specific to gram-negative bacteria, might be required for NLRP11-dependent cell death. Infection of THP-1 macrophages with the cytosolic gram-positive pathogen *Listeria monocytogenes* induced minimal levels of cell death during the experimental timeframe. Conversely, *L. monocytogenes* coated with *S. enterica* LPS induced cell death that was largely dependent on NLRP11 (Fig. 2A). The observed cell death was dependent on cytosolic localization, as *L. monocytogenes* lacking listeriolysin O (LLO), which is required to lyse the vacuole, induced minimal cell death. Introduction of LPS alone directly into the cytosol by electroporation similarly induced cell death that was significantly dependent on NLRP11, both in *NLRP11*$^{-/-}$ and NLRP11 siRNA-treated THP-1 macrophages (Fig. 2, B and C), whereas cell death induced by extracellular LPS was independent of NLRP11 (fig. S5B). As expected, upon LPS electroporation, cell death was reduced in caspase-4 null (*CASP4*$^{-/-}$) and gasdermin D null (*GSDMD*$^{-/-}$) THP-1 macrophages (fig. S5, C, D and E). The level of reduction in cell death in *CASP4*$^{-/-}$ cells

was similar to that observed for *NLRP11*$^{-/-}$ THP-1 macrophages; the greater reduction in cell death observed for *GSDMD* cells likely reflects the convergence of multiple cell death pathways on gasdermin D. Therefore, NLRP11 functions in a cell death pathway that is activated by LPS localized to the cytosol (cLPS).

NLRP11 is required for efficient activation of non-canonical inflammasome

Activation of caspase-4 was dependent on NLRP11; during *S. flexneri*, *S.* Typhimurium, or *B. thailandensis* infection, processing of caspase-4, which releases its active domains, was significantly reduced in culture supernatants of *NLRP11*$^{-/-}$ macrophages (Fig. 3, A and B, and fig. S6, A and B). The amount of pro-caspase-4 in cell lysates was unaltered by disruption of *NLRP11* (Fig. 3, A and B, and fig. S4A), indicating that the NLRP11-dependent increase in released CASP4 was not due to increased levels of protein production.

A role of the non-canonical inflammasome in *S. flexneri*-induced cell death is consistent with previously published data showing that in mouse macrophages, cell death induced by *S. flexneri* infection is reduced by 40–50% in the absence of caspase-11 (6, 20). Of note, earlier studies of *S. flexneri*-induced death of murine macrophages must be interpreted with caution, as macrophages used in these early studies lacked both caspase-1 and caspase-11 (11). Activation of gasdermin D was also significantly reduced in *NLRP11*$^{-/-}$ macrophages, yet levels of full-length gasdermin D in cell lysates were independent of NLRP11 (Fig. 3C and fig. S4, A and C). Moreover, release of the IL-1 family cytokines IL-1β and IL-18 from *S. flexneri*-infected *NLRP11*$^{-/-}$ macrophages or *NLRP11*$^{-/-}$ macrophages electroporated with LPS was impaired (fig. S7). In mouse bone marrow-derived macrophages and human epithelial cell lines, OspC3 inhibits caspase-4 processing of gasdermin D (21, 22). However, upon infection of THP-1 cells with an *ospC3* deletion *S. flexneri* strain, processing of gasdermin D was similar to that observed upon infection with wild-type *S. flexneri* (Fig. 3C).

Upon siRNA-mediated *CASP4* reduction, absence of NLRP11 caused no significant additional decrease in cell death induced by LPS electroporation (Fig. 4, A and B). Reduction in *CASP1* induced no significant decrease in cell death in response to cLPS as compared to control siRNA treatment in either *NLRP11*$^{-/-}$ or WT THP-1 macrophages (Fig. 4, A and C). Activation of caspase-1 followed a pattern parallel to that of caspase-4, with diminished processing in *NLRP11*$^{-/-}$ macrophages (fig S6, C and D). This pattern of caspase-1 activation was expected, as K+ efflux that results from activation of the non-canonical inflammasome activates NLRP3 and caspase-1 (6, 23–25). These data indicate that NLRP11 is required for efficient activation of the non-canonical inflammasome, inducing caspase-4-dependent cell death in the presence of cytosolic LPS. They also indicate that NLRP11 function in response to cytosolic LPS is largely independent of caspase-1. Also consistent with NLRP11 functioning specifically in the non-canonical inflammasome pathway, NLRP11 was not required for activation of the NLRP3 inflammasome, the NLRC4 inflammasome, or the AIM2 inflammasome (fig. S8).

NLRP11 interacts with LPS and caspase-4

In contrast to NLRP3 inflammasomes, activation of the non-canonical pathway is independent of the adaptor protein ASC (11, 14, 16). We tested whether NLRP11 interacts with other core components of the non-canonical pathway by ectopic expression of selected components in HEK293T cells, which lack most innate immune proteins, including ASC and caspase-4 (fig. S9). Biotin-conjugated LPS precipitated NLRP11 in the absence of caspase-4 (Fig. 5A), indicating that NLRP11 binds LPS independently of caspase-4. These data do not distinguish whether LPS binding to NLRP11 is direct or indirect. LPS specifically precipitated caspase-4 and its catalytically inactive derivative (CASP4 C258A), as described (14), including in the presence of NLRP11 (Fig. 5B), whereas the triacylated lipid Pam3CSK4 did not precipitate either NLRP11 or caspase-4 (Fig. 5A). In addition to binding to LPS independent of caspase-4, NLRP11 specifically and reciprocally precipitated caspase-4 (Fig. 5C and Fig. 6). Native gel electrophoresis of lysates of HEK293T cells producing FLAG-NLRP11 with or without CASP4(C258A)-Myc-FLAG and in the absence of LPS demonstrated that NLRP11 migrates at high molecular weight (more slowly than the 545 kD marker), reminiscent of NLRP3 cages (26), suggesting that within the cell, NLRP11 forms a complex independent of LPS. In addition, caspase-4 displayed an NLRP11-dependent shift in migration from low molecular weights into the higher molecular weight region in which NLRP11 migrates (Fig. 5D), consistent with formation of a high molecular weight complex that contains CASP4 and NLRP11 and which forms independent of LPS.

We developed a plate binding assay using FLAG-NLRP11 in HEK293T lysates and purified caspase-4 (fig. S10). FLAG-NLRP11 binding depended on caspase-4, as in the absence of caspase-4, bound FLAG-NLRP11 was at background levels (Fig. 5E, diamonds). Binding of NLRP11 to caspase-4 increased as a function of increasing concentrations of both NLRP11 lysate and caspase-4, resembling the asymptotic phase of a sigmoidal curve, beginning to reach saturation at 8–10 μg/ml caspase-4 coating the wells (Fig. 5E). Thus, NLRP11 separately binds LPS and caspase-4, and does so independently of ASC.

Caspase specificity of NLRP11

In addition to caspase-4, NLRP11 co-precipitated with caspase-1 but did not co-precipitate with caspase-5, a paralog of caspase-4 that binds LPS and a component of some non-canonical inflammasomes (14, 27, 28). NLRP11 also failed to co-precipitate with the more divergent human caspase-9 and only minimally with mouse caspase-11, which also binds LPS and is similar but non-identical to human caspase-4 (Fig. 6 and fig. S11). The observed interaction of NLRP11 with caspase-1 may play a role in the recently described contribution of NLRP11 to the NLRP inflammasome (29). However, NLRP11 function in cLPS-induced cell death of THP-1 macrophages is independent of caspase-1 (Fig. 4, A and C), indicating that an interaction of caspase-1 with NLRP11 contributes minimally to activation of the non-canonical inflammasome.

NLRP11 functions independently of IFNγ and guanylate-binding protein-1

Host GBPs are cytosolic proteins that bind intracellular LPS, promote non-canonical inflammasome activation (30–34), and are encoded by genes that are strongly induced

by interferon-gamma (IFNγ) (35). Human GBP1 binds LPS on the *S. flexneri* surface, whereupon it enhances caspase-4 recruitment (36). In the absence of IFNγ pre-treatment, NLRP11-dependent cell death during *S. flexneri* infection appeared to be independent of GBP1, as GBP1 was not induced by *S. flexneri* alone during the experimental timeframe (figs. S4B, and S12, A and B). IFNγ pre-treatment of THP-1 macrophages induced GBP1, as expected, yet even in the presence of GBP1, NLRP11 was required for efficient activation of *S. flexneri*-induced cell death (fig. S12, B and C). These results indicate that in THP-1 macrophages, GBP1 is likely not required for non-canonical inflammasome activation or pyroptosis or for NLRP11 function in inducing non-canonical pyroptosis, consistent with recent demonstration that GBPs are not absolutely required for *S. flexneri* induced activation of caspase-4 in epithelial cells (22). Moreover, IFNγ and GBP1 do not bypass the requirement for NLRP11 in this pathway.

In HeLa cells stably transfected with YFP-CASP4(C258S), transiently transfected Myc-NLRP11 was distributed throughout the cytosol, where it generally co-localized with YFP-CASP4(C258S) (fig. S13). In IFNγ-primed, transfected, and *S. flexneri* Δ*ipaH9.8*-infected cells, as previously described (33), puncta of CASP4(C258S) were occasionally recruited to the surface of intracellular bacteria (fig. S13C, insets). Irrespective of priming or infecting strain, NLRP11 was not observed to co-localiz with CASP4 at the bacterial surface. The lack of NLRP11 localization at the bacterial surface suggests that NLRP11 inflammasome activation does not occur at the bacterial surface, but rather elsewhere in the cytosol.

NLRP11 is required for cLPS-induced cell death in primary human macrophages

As in THP-1 macrophages, in primary human monocyte-derived macrophages, siRNA silencing of NLRP11 was associated with reduced cLPS-induced cell death (Fig. 7, A and B). Cell death depended on caspase-4 (Fig. 7, C and D), demonstrating that the requirement for NLRP11 in the non-canonical inflammasome pathway extends to primary human cells.

DISCUSSION

Here, we found that NLRP11 is required for efficient activation of the caspase-4 inflammasome in response to cLPS in human macrophages. Upon infection with intracellular gram-negative pathogens or electroporation of LPS, NLRP11 was required for efficient processing of caspase-4 and gasdermin D, release of IL-1β and IL-18, and cell death. NLRP11 co-precipitates from HEK293T lysates with LPS and separately with caspase-4.

These findings challenge the current dogma for LPS recognition – that caspase-4 is the sensor for cytosolic LPS – which is based on data that show that *in vitro* caspase-4 binds, is induced to oligomerize, and is activated by LPS (14). LPS consists of lipid A, an acylated hydrophobic diglucosamine backbone that anchors LPS in the bacterial outer membrane, core oligosaccharide, and serotype-specific O-antigen. The moiety of LPS that binds caspase-4 is lipid A (14). We speculate that caspase-4 binding and activation by LPS under the described *in vitro* conditions (14) is due, at least in part, to the presence of a multiligand platform of lipid A presented by LPS in micelles or aggregates. Like other caspases, activation of caspase-4 is triggered by proximity-induced dimerization

(14, 37–44); dimerization is sufficient to activate the caspase to undergo auto-processing, thereby releasing the small and large active subunits, which form an active heterotetrametric complex. As LPS species self-associate in micelles and aggregates at concentrations above critical micelle concentrations, estimated to be 40 nM or lower (45), and caspase-4 binds preferentially to LPS in micelles or bacterial outer membrane vesicles (46), it seems likely that LPS micelles and aggregates provide a multiligand platform for caspase-4 dimerization. Consistent with this possibility is that although at 100–250 nM, purified LPS binds, oligomerizes, and activates caspase-4 *in vitro*, in the presence of >0.25% Tween-20, LPS-mediated caspase-4 oligomerization and activation are disrupted (14).

A contribution of GBP1 to recognition of LPS in the cytosol has been described for several cell types (31, 33, 34, 36), but not for human macrophages. Moreover, GBPs are not absolutely required for activation of caspase-4 during *S. flexneri* infection of epithelial cells (22). *Shigella* spp. secrete inhibitors of GBPs, including GBP1. Consequently, the ability of NLRP11 to recognize cLPS independently of GBPs may enable human macrophages to bypass any requirement for GBPs in the control of the pathogen.

The data presented here identify NLRP11 as a primate-specific pattern recognition receptor of bacterial LPS in the cytosol of human macrophages. As such, NLRP11 is a critical component of activation of the caspase-4-dependent inflammasome and a critical mediator of caspase-4-dependent pyroptosis. Nevertheless, it is likely that delivery of high concentrations of LPS to the macrophage cytosol is sufficient to activate caspase-4 directly and independently of NLRP11, perhaps principally when multiligand LPS platforms are present. Consistent with this, a proportion of caspase-4-dependent cell death appeared to be independent of NLRP11 (Fig. 4, A and B); in these experiments, LPS was electroporated at relatively high concentration, and cells were infected with ten bacteria per cell. We speculate that NLRP11 may be particularly critical for non-canonical inflammasome activation when LPS is delivered in low amounts, such as during human infection with gram-negative pathogens, wherein the intracellular burden of organisms and free intracellular LPS, particularly with accessible lipid A moieties, is likely very low.

Limitations of the investigations presented here are that, although performed with human cells, they were *ex vivo*, and that due to the restriction of NLRP11 to primates, no mouse model for testing the relevance of NLRP11 in animals currently exists. It remains uncertain whether the unique presence of NLRP11 in primates and the absence of identifiable homologs in mice contributes to the exquisite sensitivity of humans to endotoxic shock as compared with mice: humans display ~10^4-fold increased susceptibility to gram-negative bacterial sepsis and bloodstream LPS relative to mice (47, 48). Additional insights into these relationships would facilitate much-needed improved mouse models for the study of bacterial sepsis.

MATERIALS AND METHODS

Study design.

The requirement for NLRP11 in activation of the caspase-4 inflammasome in response to gram-negative bacterial infection or LPS electroporation was assessed in THP-1

human-derived macrophages and primary human macrophages. Readouts for caspase-4 inflammasome activation included cell death (LDH release), caspase processing, and release of IL-1β and IL-18. Interactions of NLRP11 with caspases and LPS were assessed using HEK293T cells in which NLRP11 and/or caspases were expressed.

Bacterial strains and growth conditions.

Bacterial strains used in this study are listed in Table S1. *S. flexneri* strains were grown overnight in tryptic soy broth at 37°C with aeration. *L. monocytogenes* strains were grown overnight in brain heart infusion broth at 30°C at a stationary slant. *B. thailandensis* was grown overnight in low salt Luria broth (LB) at 37°C with aeration. *S. enterica* Typhimurium strains were grown in LB broth at 37°C with aeration.

Strain and plasmid construction.

The *S. flexneri ospI* deletion mutant was generated in the 2457T strain background using the lambda red method by introducing a chloramphenicol acetyltransferase (cat) cassette into the *orf169b* gene (which encodes OspI), as described (47).

pCMV6-CASP4-MYC and pCMV6-CASP5-MYC were made from pCMV6-CASP4-MYC-FLAG and pCMV6-CASP5-MYC-FLAG, gifts from S. Shin. The isoform of caspase-5 that was used was caspase-5/a, the most abundant isoform; this isoform contains nearly all sequences present in other isoforms. pCMV6-CASP4-MYC C258A and pCMV6-CASP4-MYC K19E C258A were generated by splicing by overlap extension PCR (SOE-PCR). pCMV6-CASP1-MYC C285A and pCMV6-mCASP11-MYC C254A were made from pFastBac-CASP1 C285A (gift from S. Shin) and pMSCV-mCASP11 C254A (gift from J. Kagan), respectively. pCMV6-CASP9-MYC C287S was generated by SOEing PCR from the template pET28a-CASP9 (gift from H. Wu). pMX-CMV-YFP-CASP4 C258S (31) was a gift from D. Fisch. pcDNA-NLRP11 (gift from H. Wu) was subcloned into pCMV-FLAG with an N-terminal FLAG tag for FLAG-NLRP11 and an N-terminal MYC tag for MYC-NLRP11. All FLAG tags are 3xFLAG. All N-terminal Myc tags are 6xMyc; all C-terminal Myc tags are 1xMyc. All DNA used for transfection was prepared LPS-free (Macherey-Nagel, 740410.50).

Mammalian cell culture.

All cell lines were obtained from ATCC. HEK293T cells (*Homo sapiens*, ATCC, CRL-3216, RRID:CVCL_0063) were maintained in Dulbecco's Modified Eagle's medium (Gibco, 11965118). THP-1 cells (*Homo sapiens*, ATCC, TIB-202, RRID:CVCL_0006) were maintained in RPMI-1640 (Gibco, 21870092). HeLa CCL2 cells (*Homo sapiens*, ATCC, CCL-2, RRID:CVCL_B1MH) were maintained in Dulbecco's Modified Eagle's medium (Gibco, 11965118). All media was supplemented with 10% (vol/vol) fetal bovine serum (heat inactivated, sterile filtered, R&D Systems). For THP-1 cells, RPMI-1640 media was also supplemented with 10 mM HEPES (Gibco,15630080) and 2 mM L-glutamine (Gibco, 25030081). All cells were grown at 37°C in 5% CO_2.

To differentiate monocyte cell lines into macrophage-like cells, 50 ng/mL phorbol-12-myristrate-13-acetate (PMA) was added 48 h before experiments. Where indicated, cells

were pre-treated with 2.5 or 25 U/mL IFNβ (STEMCELL Technologies, 78113) for 2 h before analysis or 10 ng/mL IFNγ (Millipore, Sigma-Aldrich, I17001) for 16–20 h prior to infection.

Generation of CRISPR knockouts.

THP-1 cells were transduced with lentivirus packaged with pLentiCas9-Blast (Addgene, 52962) generated from HEK293T cells. THP-1 cell suspensions were treated with 8 μg/mL polybrene, combined with lentivirus and centrifuged in 12-well plates for 2 h at 1000 × g at 30°C. After centrifugation, cells were incubated for 2 h and washed once with fresh media. After 48 h, blasticidin (10 μg/mL) was added to the transduced cells. Guide RNA sequence ("sgRNA3", AGGCATGCAAAGCTGTCATG) was subcloned into pLentiGuide-Puro (Addgene, 59702). Guide RNA expressing plasmids were packaged into lentivirus using HEK293T cells. Polybrene treated THP-1 cells were transduced and selected with 1 μg/mL puromycin. Cells were limiting diluted and single cell clones were screened by SURVEYOR (IDT, 706020) and Sanger sequencing coupled with TIDE analysis (49). Levels of *NLRP11* transcript in the knockout cells were determined using reverse transcriptase (RT) PCR. Cellular transcripts were prepared using RNeasy Micro Kit (Qiagen) on cells pretreated or not with 1μg/mL Pam3CSK4 for 3 h, cDNA was generated using SuperScript IV VILO kit (ThermoFisher), and PCR was performed for 40 cycles. Primers used in RT-PCR are listed in Table S2.

Generation of *TRAF6* depletion cell lines.

pLKO.1-shTRAF6 ((50), gift of A. Goldfeld), which encodes shRNA to *TRAF6*, was packaged into lentivirus in HEK293T cells. Lentivirus were introduced into NLRP11+/+ and NLRP11−/− THP-1 cell lines and cells containing pLKO.1-shTRAF6 were selected, expanded by maintenance in 0.8 μg/mL puromycin, as described (50), and stable clones were isolated by limiting dilution.

Generation of stable HeLa CCL2 cells expressing YFP-CASP4.

We generated stable HeLa CCL2 cells expressing YFP-CASP4(C258S) (31) by lentiviral transduction. Lentivirus was produced in HEK293T by transient transfection with the lentiviral backbone pMX-CMV-YFP CASP4(C258S) and the three packaging plasmids pVSV-G (#138479, Addgene), pAdvantage (E1711, Promega), and pGag-Pol (#14887, Addgene). DNA, mixed with FuGENE 6 Transfection Reagent (Promega) in Opti-MEM (Gibco), was incubated at RT for 15 min, then added dropwise into HEK293T cells. After 48h, the supernatant containing the lentivirus was collected, filtered using a 0.45 μm membrane filter, and supplemented with polybrene (Sigma) at 8 μg/mL. Lentivirus was then transduced into HeLa CCL2 cells by centrifugation of the HEK293T supernatant for 2 h at 1000 × g at 30°C. Two days later, HeLa CCL2 containing YFP-CASP4(C258S) were selected and maintained with 2 μg/mL of puromycin.

Precipitation experiments.

HEK293T cells were transiently transfected using Fugene6 (Promega). A stock solution of 10x Buffer A (100 mM HEPES, 1500 mM NaCl, 10 mM EGTA, 1 mM $MgCl_2$, pH 7.4)

was prepared. The cell culture medium was removed 24–48 h after transfection. Cells were washed with cold PBS and lysed in 1x Buffer A, 0.5% Triton-X. Cell lysates were incubated on ice for 15 min, vortexed for 15 s and centrifuged at 13,200 rpm for 10 min at 4°C. The pellet was discarded, and Bradford assay was used to determine protein concentration. 30 μL of FLAG M2 Magnetic Beads (Millipore-Sigma, M8823) were washed twice in 1x Buffer A, 0.1% Triton-X and equilibrated in the same buffer at 4°C for 2 h. 500 μg of protein lysate was incubated with the beads for 2 h at 4°C. Beads were washed 3 times with 1x Buffer A, 0.1% Triton-X and eluted with 50 μL of 2x Laemmli buffer.

Streptavidin pulldown was largely as described (14), with minor modifications. Cell lysates were diluted to 4 mg/mL before a 2 h incubation with beads. For co-precipitation experiments, separate cells were transfected with each DNA construct, and pre-specified amounts of lysates were combined with each other or with untransfected lysate, such that the total amount of lysate were similar in each experimental condition; these lysates were then incubated at 37°C overnight. To reduce non-specific binding, lysates were pre-cleared with streptavidin beads and then were incubated for 2 h at 30°C with 4 μg biotinylated *E. coli* O111:B4 LPS loaded onto 8 μg of Streptavidin Mag sepharose (GE, 28985738, or Pierce, 88816).

Native gel electrophoresis.

2.4×10^6 HEK293T cells were transiently transfected with 3.5 μg of pCMV-FLAG-NLRP11, 5.5 μg of pCMV-CASP4(C258S)-Myc-FLAG or a combination of both, using Fugene6 (Promega). 48 h after transfection, the cell culture medium was removed, and cells were washed with cold PBS and collected into sample buffer for native PAGE (NativePAGE™ Sample Prep Kit, ThermoFisher BN2008). Before loading the samples, 0.125% digitonin and 0.031% G-250 dye were added to the cells in sample buffer. 20 μL of sample and non-denaturing molecular weight 14–500 kDa (Sigma, MWND500–1KT) were loaded in a native gel (NativePAGE™ 3 to 12%, Bis-Tris, 1.0 mm, Mini Protein Gels, ThermoFisher BN1001BOX) and run for 4 h.

Plate binding assays.

Clear flat bottom Nunc Maxisorp ELISA plates (Thermo Fisher, 442404) were coated with various concentrations of purified recombinant caspase-4 (Origene, TP760359) overnight at 4°C. The plates were washed 3x with PBS then blocked for 2 h at RT with 1% bovine serum albumin (Fisher, BP9700100) in PBS. Excess blocking solution was removed. HEK 293T cells transiently expressing FLAG-NLRP11 and control untransfected cells were lysed in 50 mM Tris-HCl pH 7.4, 150 mM NaCl, 5 mM $MgCl_2$, 100 μg/ml digitonin (Thermo Fisher Scientific, BN2006) and complete Mini EDTA-free protease inhibitor (Roche), as described (33). Total protein concentration of lysates was normalized to 2 mg/mL. Serial dilutions were in untransfected HEK293T cell lysate. Varying concentrations of cell lysates were incubated with pre-blocked ELISA plates for 1 h at RT. Excess lysate was removed by washing 3 times with PBS. For detection of FLAG-NLRP11, wells were incubated with 0.8 μg/mL anti-FLAG rabbit (Sigma, F7425, RRID:AB_439687) for 1 h at RT, and after washing with PBS, 0.16 μg/mL goat-anti-rabbit conjugated to horseradish peroxidase (HRP) (Jackson ImmunoResearch Labs, 111–035-144, RRID:AB_2307391). To detect caspase-4

bound to the plate, wells were incubated with 0.5 μg/mL anti-caspase-4 (Santa Cruz, sc-56056, RRID:AB_781828) and, after washing with PBS, 0.16 μg/mL goat-anti-mouse conjugated to HRP (Jackson ImmunoResearch Labs, 115–035-003, RRID:AB_10015289), each for 1 hr. After 6 washes with PBS, 50 μL of One Step Ultra-TMB (Fisher Scientific, PI34029) was added to each well and incubated for 5 min before stopping with 4 N sulfuric acid and reading in a BioTek plate reader.

Bacterial infection.

Overnight cultures were started from a single colony taken from a freshly streaked plate. Infections with *S. flexneri* were performed with exponential phase bacteria, after back-dilution from overnight cultures. Infections with *L. monocytogenes* were performed with stationary phase bacteria from overnight cultures. Infections were performed with a multiplicity of infection (MOI) of 10 for *S. flexneri* cultures and 1 for *L. monocytogenes*. For *L. monocytogenes* infections, bacteria were mixed with 10 ug/ml LPS or no LPS in a volume of 1 ml just prior to infection of the cells (13). Bacteria were centrifuged onto cells at 2000 rpm for 10 min, followed by incubation at 37°C. After 30 min, the cells were washed twice, and then 25 μg/mL gentamicin was added to the media to kill extracellular bacteria. To determine efficiency of bacterial invasion, cells were harvested with trypsin 20 minutes later and lysed with 0.5% Triton X-100, and lysates were plated for bacterial counts. Where appropriate, *S. enterica* serovar Minnesota LPS was added to 10 μg/mL at the time of infection and MCC950 to 1 μM 30 min prior to infection and maintained during infection.

For LDH assays of *S. flexneri* infected cells, 100 μL of cell culture supernatant was collected at 2 h and 30 min and at 5 h and/or 30 min of infection; for detection of caspases and/or gasdermin D by western blot, 100 μL of cell culture supernatant was collected at the same time points and was mixed with 35 μL 4x Laemmli buffer supplemented with cOmplete EDTA-free protease inhibitors (Roche, 5056489001).

For parallel analyses of *L. monocytogenes* infected cells, gentamicin was used at 15–25 μg/mL; for analysis of *L. monocytogenes* delivery of LPS to the cytosol, samples were collected at 6 h of infection, and for analysis of *L. monocytogenes* presentation of NLRC4 ligands PrgJ and FlaA, samples were collected at 16 h of infection. For western blot analyses, whole cell lysates were collected in 2x Laemmli buffer.

Infections with *B. thailandensis* and *S.* Typhimurium were performed with exponential phase bacteria at a multiplicity of infection (MOI) of 10. Bacteria were centrifuged onto cells at 2000 rpm for 10 min, followed by incubation at 37°C. For *S.* Typhimurium, after 30 min incubation, the cells were washed twice, and then 25 μg/mL gentamicin was added to the media to kill extracellular bacteria. For *B. thailandensis*, after 2 h incubation, the cells were washed twice with cRPMI. For LDH assays with *S.* Typhimurium infection, 100 μL of cell culture supernatant was collected at 5 h 30 min to 7 h 30 min of infection and, for LDH assays with *B. thailandensis*, 100 μL of cell culture supernatant was collected at 24 h.

Isolation of primary human peripheral blood mononuclear cells (PBMCs) and CD14 monocytes.

Cells were isolated from leukopaks from individual healthy human donors (Crimson Core Laboratories, Brigham and Women's Hospital) using density-gradient centrifugation. Briefly, blood was diluted 1:2 with RPMI-1640 (Gibco), layered on top of Ficoll-Paque Plus (GE Healthcare) using SepMate™−50 (IVD) (StemCell Technologies), and centrifuged at 1,200g for 20 min. The PBMC layer was collected and resuspended in 50 ml RPMI-1640 (Gibco) and centrifuged again at 300 g for 10 min. The cells were counted, resuspended in Cryostor CS10 (StemCell Technologies), and aliquoted in cryopreservation tubes at a concentration of 1×10^8 cells per mL. The tubes were placed at −80°C overnight, then transferred to liquid nitrogen for long-term storage. To isolate CD14+ cells, EasySep™ Human CD14 Positive Selection Kit II (StemCell Technologies) was used, following the manufacturer's instructions. Cells were cultured in complete RPMI, differentiated with 25 ng/mL m-CSF (StemCell Technologies), and maintained at 37°C in 5% CO_2.

LPS electroporation.

Electroporation of cells with LPS was performed, as previously described (14), using the Neon Transfection System (Invitrogen) according to the manufacturer's instructions using *S.* Minnesota LPS at indicated concentrations. THP-1 cells were seeded in low-attachment 10 cm dishes with 50 ng/mL PMA in RPMI. After 48 h, the cells were lifted in PBS (without calcium or magnesium). For electroporation, 1.5×10^6 THP-1 cells were pelleted, resuspended in Resuspension Buffer R with 2 μg LPS per 10^6 cells or water control. Using a 10 μL Neon tip, cells were pulsed once at 1400 V and 10 ms pulse width. For primary human macrophage cells, 7.5×10^5 CD14 macrophages were pelleted, then resuspended in Resuspension Buffer T with LPS, as above, or water control. Using a 10 μL Neon tip, cells were pulsed 2 times at 2250 V and 20 ms pulse width. Electroporated cells were immediately resuspended in 2 mL of RPMI and placed into wells of a 24 well plate. Cells were incubated for 2.5 h at 37°C before measuring LDH release.

siRNA transient knockdowns.

siRNAs used for NLRP11 knockdowns were Hs_NALP11_1 FlexiTube siRNA and Hs_NALP11_5 FlexiTube siRNA at 10 nM total (5 nM each siRNA); for caspase-4 knockdowns were 3941, 4036 and 4130 at 30 nM total (10 nM each siRNA) (ThermoFisher); and for Caspase-1 Hs_CASP1_14 FlexiTube siRNA and Hs_CASP1_13 FlexiTube siRNA at 30 nM total (15 nM each siRNA). AllStars Negative Control siRNAs (Qiagen) were used as negative controls at 10 nM or 30 nM, accordingly. In each set of experiments, to control for loading, an identical number of cells were used and processed for each experimental condition. siRNAs were transfected using the HiPerfect reagent (Qiagen) into primary human monocyte-derived macrophages 72 h before or into THP-1 cells 48 h before experimental assays, following the manufacturer's protocol for "Transfection of Differentiated Macrophage Cell Lines." After transfection, cells were maintained at 37°C in 5% CO_2. Degree of knock-down of caspases was assessed by western blot of lysates of equivalent numbers of cells for each condition.

Assessment of transcript levels.

To determine levels of *NLRP11*, *CASP4*, and *GSDMD* transcripts, either at baseline or following siRNA, reverse transcription followed by real-time quantitative PCR (RT-qPCR) was performed using SuperScript IV VILO Master Mix (ThermoFisher Scientific, 11756050), SsoFast EvaGreen Supermix (BioRad, #172–5201), and the QuantStudio™ 5 Real-Time PCR System, 384-well, real-time PCR detection system (Applied Biosystems, A28140) with cycles of 30 s at 95°C, followed by 40 cycles of 5 s at 95°C and 20–30 s at 60°C. Relative expression levels were calculated using the manufacturer's software for double delta threshold cycle (Ct) method (Design and Analysis Software 2.6.0, Applied Biosystems), using transcripts from housekeeping genes *ACTB* and *GAPDH* (for *CASP4* and *GSDMD*) and *HPRT1* (for *NLRP11*). Primers used in RT-qPCR are listed in Table S2.

LDH assay and cytokine ELISAs.

LDH was measured using an LDH Cytotoxicity Kit (Pierce, 88953), CyQUANT™ LDH Cytotoxicity Assay (Invitrogen C2030), or Cytotoxicity Detection Kit (Sigma, 11644793001) per the manufacturer's instructions; for any set of experiments, the same assay kit was used for all experiments. Measurements at 490 nm and 680 nm were taken immediately after the addition of Stop Solution using a BioTek Plate Reader. To determine LDH activity, the 680 nm absorbance value (background) was subtracted from the 490-nm absorbance value, and cytotoxicity was calculated for each sample as LDH activity as a fraction of the total LDH activity for cells treated with the Triton X-100 lysis buffer provided by the manufacturer. For experiments involving primary cells, a different donor was used for each biological replicate; due to inherent variability from donor to donor in the baseline levels of death in cell death assays, within-donor data were normalized to the negative control condition before compilation of the biological replicates. Assays of levels of secreted cytokines were performed using the Human Total IL-18 DuoSet ELISA (R&D Biosystems, DY318–05), ELISA MAX Deluxe Set Human IL-1α (Biolegend, 445804), and ELISA MAX Deluxe Set Human IL-1β (Biolegend, 437004), per the manufacturer's instructions.

Immunofluorescence microscopy of intracellular Myc-NLRP11.

HeLa CCL2 stably transfected with YFP-CASP4(C258S) were transiently transfected with Myc-NLRP11 using 6 ug DNA and 15 μL FuGENE 6 (Fisher Scientific, E2692) per 2×10^5 cells per well on coverslips in a 6-well plate with or without IFNγ priming. After 24 h, cells were infected for 1 h with *S. flexneri* as described in Methods (Bacterial Infection) with slight modification. Bacteria were not centrifuged onto the cells; therefore, to increase the efficiency of infection in the absence of centrifugation, the bacterial strains used carried the AFA-I pilus (51). Infected cells were fixed for 20 min at RT with 4% paraformaldehyde in PBS, washed with PBS, permeabilized for 7 min. at RT with 0.1% Triton X-100, washed with PBS, blocked for 30 min at RT with 10% goat serum (Sigma, G6767), labeled for 45 min at RT with c-Myc and *Shigella* primary antibodies and Hoechst 3342 (16.2 uM, Tocris, 5117), washed with PBS, labeled for 45 min at RT with donkey anti-mouse Alexa Flour 594 highly cross-adsorbed and goat anti-rabbit Alexa Fluor 647 highly cross-adsorbed, and

mounted onto slides with ProLong Diamond Mounting Media (Fisher, P36970), maintaining the coverslips in the dark throughout.

Confocal imaging was performed using a Nikon Ti inverted microscope with Yokogawa CSU-W1 single disk (50 μm pinhole size) spinning disk confocal unit and equipped with a Nikon linear-encoded motorized stage with a PI 250 nm range Z piezo insert and an Andor Zyla 4.2 plus sCMOS monochrome camera using a Plan Apo λ 100x/1.45 Oil DIC oil immersion objective with Cargille Type 37 immersion oil. Green, red, blue and far-red fluorescence were collected by illuminating the sample with solid-state directly modulated 488 nm, 561 nm, 405 nm, and 640 nm laser lines in a Toptica iChrome MLE laser launch, respectively. Nikon Elements AR 5.02 acquisition software was used to acquire the data.

Antibodies.

NLRP11 (NALP11, Invitrogen, PA5–21026, RRID:AB_11152984) rabbit polyclonal antibody was used at 1 μg/mL (1:1000). Caspase-1 (Abcam, ab207802, RRID:AB_2889889) rabbit monoclonal antibody was used at 0.5 μg/mL (1:1000). Caspase-4 (Santa Cruz, sc-56056, RRID:AB_781828), and gasdermin D (Santa Cruz, sc-81868, RRID:AB_2263768) mouse monoclonal antibodies were used at 0.5 μg/mL (1:200). FLAG M2 mouse monoclonal antibody (Sigma, F3165, RRID:AB_259529) was used at 76 ng/mL (1:5000). Myc rabbit monoclonal antibody (Cell Signaling, 2278, RRID:AB_490778) was used at 1:1000. GBP1 mouse monoclonal antibody (Abcam, ab119236, RRID:AB_10900135) was used at 1:1000. GBP2 mouse monoclonal antibody (Santa Cruz, sc-271568, RRID:AB_10655677) was used at 1:200. Rabbit STAT1 antibody (Cell Signaling Technology, 9172, RRID:AB_2198300) was used at 32 ng/mL, and rabbit phospho-STAT1 (Tyr-701) antibody (Cell Signaling Technology, 9167, RRID:AB_561284) was used at 59 ng/mL.

For western blots of immunoprecipitations, the secondary antibody used was TrueBlot horseradish peroxidase-conjugated anti-mouse Ig (Rockland, 18–8817-31, RRID:AB_2610850). For detecting β-actin, horseradish peroxidase-conjugated anti-β-actin antibody (Sigma, A3854, RRID:AB_262011) was used. For all other western blots, the secondary antibody used was horseradish peroxidase-conjugated goat anti-rabbit or goat anti-mouse IgG antibodies (Jackson ImmunoResearch, 115–035-003, RRID:AB_10015289, or 111–035-144, RRID:AB_2307391). All antibodies were diluted in 5% milk in PBS with 0.05% Tween-20.

For immunofluorescence microscopy, c-Myc mouse monoclonal antibody (Takara Bio, 631206, RRID:AB_2928131) was used at 4 μg/mL (1:50), *Shigella* rabbit polyclonal antibody (Abcam ab65282, RRID:AB_1142846) was used at 20 μg/mL (1:200), Alexa Fluor 594 donkey anti-mouse antibody (Invitrogen, A21203, RRID:AB_141633) was used at 10 μg/mL (1:200), and Alexa Fluor 647 goat anti-rabbit antibody (Invitrogen, A32733, RRID:AB_2633282) was used at 10 μg/mL (1:200).

Statistical analysis.

Unless otherwise indicated, all results are data from at least 3 independent biological replicates. On bar graphs, each individual symbol is data from an independent biological

replicate. The methods used for statistical analysis of significance are indicated in the figure legends. All analysis was performed with Prism version 9.

Supplementary Material

Refer to Web version on PubMed Central for supplementary material.

Acknowledgments:

We thank Jonathan Kagan, Hao Wu, Kate Fitzgerald, Sunny Shin, Ann Goldfeld, Margaret Kielian, Peggy Cotter, Jeffrey Miller, Daniel Portnoy, Cammie Lesser, and Daniel Fisch for reagents, and the MicRoN Microscopy core at Harvard Medical School for imaging assistance.

Funding:

This research was supported by Real Colegio Complutense Fellowship, Real Colegio Complutense at Harvard (MLGM), National Institutes of Health grant R01 AI081724 (MBG), National Institutes of Health grant R01 AI173030 (MBG), National Institutes of Health grant F32 AI145128 (ASZ), National Institutes of Health grant F32 AI126765 (KAM), and National Institutes of Health grant T32 AI007061 (ASZ).

Data and materials availability:

All data needed to support the conclusions of the paper are present in the paper or the Supplementary Materials. All materials are available by request to M.B.G., restricted by institutional MTAs.

References and Notes:

1. Brewer SM, Brubaker SW, Monack DM, Host inflammasome defense mechanisms and bacterial pathogen evasion strategies. Curr Opin Immunol 60, 63–70 (2019). [PubMed: 31174046]
2. Broz P, Dixit VM, Inflammasomes: mechanism of assembly, regulation and signalling. Nat Rev Immunol 16, 407–420 (2016). [PubMed: 27291964]
3. Jorgensen I, Rayamajhi M, Miao EA, Programmed cell death as a defence against infection. Nat Rev Immunol 17, 151–164 (2017). [PubMed: 28138137]
4. Wright SS, Vasudevan SO, Rathinam VA, Mechanisms and Consequences of Noncanonical Inflammasome-Mediated Pyroptosis. J Mol Biol, 167245 (2021).
5. Deets KA, Vance RE, Inflammasomes and adaptive immune responses. Nat Immunol 22, 412–422 (2021). [PubMed: 33603227]
6. Kayagaki N, Stowe IB, Lee BL, O'Rourke K, Anderson K, Warming S, Cuellar T, Haley B, Roose-Girma M, Phung QT, Liu PS, Lill JR, Li H, Wu J, Kummerfeld S, Zhang J, Lee WP, Snipas SJ, Salvesen GS, Morris LX, Fitzgerald L, Zhang Y, Bertram EM, Goodnow CC, Dixit VM, Caspase-11 cleaves gasdermin D for non-canonical inflammasome signalling. Nature 526, 666–671 (2015). [PubMed: 26375259]
7. Shi J, Zhao Y, Wang K, Shi X, Wang Y, Huang H, Zhuang Y, Cai T, Wang F, Shao F, Cleavage of GSDMD by inflammatory caspases determines pyroptotic cell death. Nature 526, 660–665 (2015). [PubMed: 26375003]
8. Ding J, Wang K, Liu W, She Y, Sun Q, Shi J, Sun H, Wang DC, Shao F, Pore-forming activity and structural autoinhibition of the gasdermin family. Nature 535, 111–116 (2016). [PubMed: 27281216]
9. He WT, Wan H, Hu L, Chen P, Wang X, Huang Z, Yang ZH, Zhong CQ, Han J, Gasdermin D is an executor of pyroptosis and required for interleukin-1beta secretion. Cell Res 25, 1285–1298 (2015). [PubMed: 26611636]

10. Liu X, Zhang Z, Ruan J, Pan Y, Magupalli VG, Wu H, Lieberman J, Inflammasome-activated gasdermin D causes pyroptosis by forming membrane pores. Nature 535, 153–158 (2016). [PubMed: 27383986]
11. Kayagaki N, Warming S, Lamkanfi M, Vande Walle L, Louie S, Dong J, Newton K, Qu Y, Liu J, Heldens S, Zhang J, Lee WP, Roose-Girma M, Dixit VM, Non-canonical inflammasome activation targets caspase-11. Nature 479, 117–121 (2011). [PubMed: 22002608]
12. Kayagaki N, Wong MT, Stowe IB, Ramani SR, Gonzalez LC, Akashi-Takamura S, Miyake K, Zhang J, Lee WP, Muszynski A, Forsberg LS, Carlson RW, Dixit VM, Noncanonical inflammasome activation by intracellular LPS independent of TLR4. Science 341, 1246–1249 (2013). [PubMed: 23887873]
13. Hagar JA, Powell DA, Aachoui Y, Ernst RK, Miao EA, Cytoplasmic LPS activates caspase-11: implications in TLR4-independent endotoxic shock. Science 341, 1250–1253 (2013). [PubMed: 24031018]
14. Shi J, Zhao Y, Wang Y, Gao W, Ding J, Li P, Hu L, Shao F, Inflammatory caspases are innate immune receptors for intracellular LPS. Nature 514, 187–192 (2014). [PubMed: 25119034]
15. Russo BC, Stamm LM, Raaben M, Kim CM, Kahoud E, Robinson LR, Bose S, Queiroz AL, Herrera BB, Baxt LA, Mor-Vaknin N, Fu Y, Molina G, Markovitz DM, Whelan SP, Goldberg MB, Intermediate filaments enable pathogen docking to trigger type 3 effector translocation. Nat Microbiol 1, 16025 (2016). [PubMed: 27572444]
16. Ellwanger K, Becker E, Kienes I, Sowa A, Postma Y, Cardona Gloria Y, Weber ANR, Kufer TA, The NLR family pyrin domain-containing 11 protein contributes to the regulation of inflammatory signaling. The Journal of biological chemistry 293, 2701–2710 (2018). [PubMed: 29301940]
17. Wu C, Su Z, Lin M, Ou J, Zhao W, Cui J, Wang RF, NLRP11 attenuates Toll-like receptor signalling by targeting TRAF6 for degradation via the ubiquitin ligase RNF19A. Nat Commun 8, 1977 (2017). [PubMed: 29215004]
18. Qin Y, Su Z, Wu Y, Wu C, Jin S, Xie W, Jiang W, Zhou R, Cui J, NLRP11 disrupts MAVS signalosome to inhibit type I interferon signaling and virus-induced apoptosis. EMBO Rep 18, 2160–2171 (2017). [PubMed: 29097393]
19. Sanada T, Kim M, Mimuro H, Suzuki M, Ogawa M, Oyama A, Ashida H, Kobayashi T, Koyama T, Nagai S, Shibata Y, Gohda J, Inoue J, Mizushima T, Sasakawa C, The Shigella flexneri effector OspI deamidates UBC13 to dampen the inflammatory response. Nature 483, 623–626 (2012). [PubMed: 22407319]
20. Napier BA, Brubaker SW, Sweeney TE, Monette P, Rothmeier GH, Gertsvolf NA, Puschnik A, Carette JE, Khatri P, Monack DM, Complement pathway amplifies caspase-11-dependent cell death and endotoxin-induced sepsis severity. J Exp Med 213, 2365–2382 (2016). [PubMed: 27697835]
21. Kobayashi T, Ogawa M, Sanada T, Mimuro H, Kim M, Ashida H, Akakura R, Yoshida M, Kawalec M, Reichhart JM, Mizushima T, Sasakawa C, The Shigella OspC3 effector inhibits caspase-4, antagonizes inflammatory cell death, and promotes epithelial infection. Cell host & microbe 13, 570–583 (2013). [PubMed: 23684308]
22. Li Z, Liu W, Fu J, Cheng S, Xu Y, Wang Z, Liu X, Shi X, Liu Y, Qi X, Liu X, Ding J, Shao F, Shigella evades pyroptosis by arginine ADP-riboxanation of caspase-11. Nature 599, 290–295 (2021). [PubMed: 34671164]
23. Ruhl S, Broz P, Caspase-11 activates a canonical NLRP3 inflammasome by promoting K(+) efflux. Eur J Immunol 45, 2927–2936 (2015). [PubMed: 26173909]
24. Schmid-Burgk JL, Gaidt MM, Schmidt T, Ebert TS, Bartok E, Hornung V, Caspase-4 mediates non-canonical activation of the NLRP3 inflammasome in human myeloid cells. Eur J Immunol 45, 2911–2917 (2015). [PubMed: 26174085]
25. Rathinam VA, Vanaja SK, Waggoner L, Sokolovska A, Becker C, Stuart LM, Leong JM, Fitzgerald KA, TRIF licenses caspase-11-dependent NLRP3 inflammasome activation by gram-negative bacteria. Cell 150, 606–619 (2012). [PubMed: 22819539]
26. Andreeva L, David L, Rawson S, Shen C, Pasricha T, Pelegrin P, Wu H, NLRP3 cages revealed by full-length mouse NLRP3 structure control pathway activation. Cell 184, 6299–6312 e6222 (2021). [PubMed: 34861190]

27. Baker PJ, Boucher D, Bierschenk D, Tebartz C, Whitney PG, D'Silva DB, Tanzer MC, Monteleone M, Robertson AA, Cooper MA, Alvarez-Diaz S, Herold MJ, Bedoui S, Schroder K, Masters SL, NLRP3 inflammasome activation downstream of cytoplasmic LPS recognition by both caspase-4 and caspase-5. Eur J Immunol 45, 2918–2926 (2015). [PubMed: 26173988]
28. Bitto NJ, Baker PJ, Dowling JK, Wray-McCann G, De Paoli A, Tran LS, Leung PL, Stacey KJ, Mansell A, Masters SL, Ferrero RL, Membrane vesicles from Pseudomonas aeruginosa activate the noncanonical inflammasome through caspase-5 in human monocytes. Immunol Cell Biol 96, 1120–1130 (2018). [PubMed: 30003588]
29. Gangopadhyay A, Devi S, Tenguria S, Carriere J, Nguyen H, Jager E, Khatri H, Chu LH, Ratsimandresey RA, Dorfleutner A, Stehlik C, NLRP3 licenses NLRP11 for inflammasome activation in human macrophages. Nat Immunol 23, 892–903 (2022). [PubMed: 35624206]
30. Pilla DM, Hagar JA, Haldar AK, Mason AK, Degrandi D, Pfeffer K, Ernst RK, Yamamoto M, Miao EA, Coers J, Guanylate binding proteins promote caspase-11-dependent pyroptosis in response to cytoplasmic LPS. Proc Natl Acad Sci U S A 111, 6046–6051 (2014). [PubMed: 24715728]
31. Fisch D, Bando H, Clough B, Hornung V, Yamamoto M, Shenoy AR, Frickel EM, Human GBP1 is a microbe-specific gatekeeper of macrophage apoptosis and pyroptosis. The EMBO journal 38, e100926 (2019). [PubMed: 31268602]
32. Santos JC, Dick MS, Lagrange B, Degrandi D, Pfeffer K, Yamamoto M, Meunier E, Pelczar P, Henry T, Broz P, LPS targets host guanylate-binding proteins to the bacterial outer membrane for non-canonical inflammasome activation. The EMBO journal 37, (2018).
33. Wandel MP, Kim BH, Park ES, Boyle KB, Nayak K, Lagrange B, Herod A, Henry T, Zilbauer M, Rohde J, MacMicking JD, Randow F, Guanylate-binding proteins convert cytosolic bacteria into caspase-4 signaling platforms. Nat Immunol 21, 880–891 (2020). [PubMed: 32541830]
34. Santos JC, Boucher D, Schneider LK, Demarco B, Dilucca M, Shkarina K, Heilig R, Chen KW, Lim RYH, Broz P, Human GBP1 binds LPS to initiate assembly of a caspase-4 activating platform on cytosolic bacteria. Nat Commun 11, 3276 (2020). [PubMed: 32581219]
35. Kim BH, Shenoy AR, Kumar P, Bradfield CJ, MacMicking JD, IFN-inducible GTPases in host cell defense. Cell host & microbe 12, 432–444 (2012). [PubMed: 23084913]
36. Kutsch M, Sistemich L, Lesser CF, Goldberg MB, Herrmann C, Coers J, Direct binding of polymeric GBP1 to LPS disrupts bacterial cell envelope functions. The EMBO journal 39, e104926 (2020). [PubMed: 32510692]
37. Poyet JL, Srinivasula SM, Tnani M, Razmara M, Fernandes-Alnemri T, Alnemri ES, Identification of Ipaf, a human caspase-1-activating protein related to Apaf-1. The Journal of biological chemistry 276, 28309–28313 (2001). [PubMed: 11390368]
38. Pop C, Timmer J, Sperandio S, Salvesen GS, The apoptosome activates caspase-9 by dimerization. Mol Cell 22, 269–275 (2006). [PubMed: 16630894]
39. MacCorkle RA, Freeman KW, Spencer DM, Synthetic activation of caspases: artificial death switches. Proc Natl Acad Sci U S A 95, 3655–3660 (1998). [PubMed: 9520421]
40. Faustin B, Lartigue L, Bruey JM, Luciano F, Sergienko E, Bailly-Maitre B, Volkmann N, Hanein D, Rouiller I, Reed JC, Reconstituted NALP1 inflammasome reveals two-step mechanism of caspase-1 activation. Mol Cell 25, 713–724 (2007). [PubMed: 17349957]
41. Baliga BC, Read SH, Kumar S, The biochemical mechanism of caspase-2 activation. Cell Death Differ 11, 1234–1241 (2004). [PubMed: 15297885]
42. Karki P, Dahal GR, Park IS, Both dimerization and interdomain processing are essential for caspase-4 activation. Biochemical and biophysical research communications 356, 1056–1061 (2007). [PubMed: 17400183]
43. Wang K, Sun Q, Zhong X, Zeng M, Zeng H, Shi X, Li Z, Wang Y, Zhao Q, Shao F, Ding J, Structural Mechanism for GSDMD Targeting by Autoprocessed Caspases in Pyroptosis. Cell 180, 941–955 e920 (2020). [PubMed: 32109412]
44. Yin Q, Park HH, Chung JY, Lin SC, Lo YC, da Graca LS, Jiang X, Wu H, Caspase-9 holoenzyme is a specific and optimal procaspase-3 processing machine. Mol Cell 22, 259–268 (2006). [PubMed: 16630893]

45. Sasaki H, White SH, Aggregation behavior of an ultra-pure lipopolysaccharide that stimulates TLR-4 receptors. Biophys J 95, 986–993 (2008). [PubMed: 18375521]
46. Wacker MA, Teghanemt A, Weiss JP, Barker JH, High-affinity caspase-4 binding to LPS presented as high molecular mass aggregates or in outer membrane vesicles. Innate Immun 23, 336–344 (2017). [PubMed: 28409545]
47. Taveira da Silva AM, Kaulbach HC, Chuidian FS, Lambert DR, Suffredini AF, Danner RL, Brief report: shock and multiple-organ dysfunction after self-administration of Salmonella endotoxin. N Engl J Med 328, 1457–1460 (1993). [PubMed: 8479465]
48. Schaedler RW, Dubos RJ, The susceptibility of mice to bacterial endotoxins. J Exp Med 113, 559–570 (1961). [PubMed: 13747161]
49. Brinkman EK, Chen T, Amendola M, van Steensel B, Easy quantitative assessment of genome editing by sequence trace decomposition. Nucleic Acids Res 42, e168 (2014). [PubMed: 25300484]
50. Ranjbar S, Jasenosky LD, Chow N, Goldfeld AE, Regulation of Mycobacterium tuberculosis-dependent HIV-1 transcription reveals a new role for NFAT5 in the toll-like receptor pathway. PLoS Pathog 8, e1002620 (2012). [PubMed: 22496647]
51. Labigne-Roussel AF, Lark D, Schoolnik G, Falkow S, Cloning and expression of an afimbrial adhesin (AFA-I) responsible for P blood group-independent, mannose-resistant hemagglutination from a pyelonephritic Escherichia coli strain. Infect Immun 46, 251–259 (1984). [PubMed: 6148308]
52. Labrec EH, Schneider H, Magnani TJ, Formal SB, Epithelial Cell Penetration as an Essential Step in the Pathogenesis of Bacillary Dysentery. J Bacteriol 88, 1503–1518 (1964). [PubMed: 16562000]
53. Wing HJ, Yan AW, Goldman SR, Goldberg MB, Regulation of IcsP, the outer membrane protease of the Shigella actin tail assembly protein IcsA, by virulence plasmid regulators VirF and VirB. J Bacteriol 186, 699–705 (2004). [PubMed: 14729695]
54. Miller KA, Garza-Mayers AC, Leung Y, Goldberg MB, Identification of interactions among host and bacterial proteins and evaluation of their role early during Shigella flexneri infection. Microbiology (Reading) 164, 540–550 (2018). [PubMed: 29488864]
55. Maurelli AT, Blackmon B, Curtiss R 3rd, Loss of pigmentation in Shigella flexneri 2a is correlated with loss of virulence and virulence-associated plasmid. Infect Immun 43, 397–401 (1984). [PubMed: 6360906]
56. Piro AS, Hernandez D, Luoma S, Feeley EM, Finethy R, Yirga A, Frickel EM, Lesser CF, Coers J, Detection of Cytosolic Shigella flexneri via a C-Terminal Triple-Arginine Motif of GBP1 Inhibits Actin-Based Motility. mBio 8, (2017).
57. Novem V, Shui G, Wang D, Bendt AK, Sim SH, Liu Y, Thong TW, Sivalingam SP, Ooi EE, Wenk MR, Tan G, Structural and biological diversity of lipopolysaccharides from Burkholderia pseudomallei and Burkholderia thailandensis. Clin Vaccine Immunol 16, 1420–1428 (2009). [PubMed: 19692625]
58. Gedde MM, Higgins DE, Tilney LG, Portnoy DA, Role of listeriolysin O in cell-to-cell spread of Listeria monocytogenes. Infect Immun 68, 999–1003 (2000). [PubMed: 10639481]
59. Sauer JD, Pereyre S, Archer KA, Burke TP, Hanson B, Lauer P, Portnoy DA, Listeria monocytogenes engineered to activate the Nlrc4 inflammasome are severely attenuated and are poor inducers of protective immunity. Proc Natl Acad Sci U S A 108, 12419–12424 (2011). [PubMed: 21746921]
60. Tsuchiya K, Nakajima S, Hosojima S, Thi Nguyen D, Hattori T, Manh Le T, Hori O, Mahib MR, Yamaguchi Y, Miura M, Kinoshita T, Kushiyama H, Sakurai M, Shiroishi T, Suda T, Caspase-1 initiates apoptosis in the absence of gasdermin D. Nat Commun 10, 2091 (2019). [PubMed: 31064994]
61. Maess MB, Sendelbach S, Lorkowski S, Selection of reliable reference genes during THP-1 monocyte differentiation into macrophages. BMC Mol Biol 11, 90 (2010). [PubMed: 21122122]
62. Casson CN, Yu J, Reyes VM, Taschuk FO, Yadav A, Copenhaver AM, Nyguyen HT, Collman RG, Shin S, Human caspase-4 mediates noncanonical inflammasome activation against gram-negative bacterial pathogens. Proc Natl Acad Sci U S A 112, 6688–6693 (2015). [PubMed: 25964352]

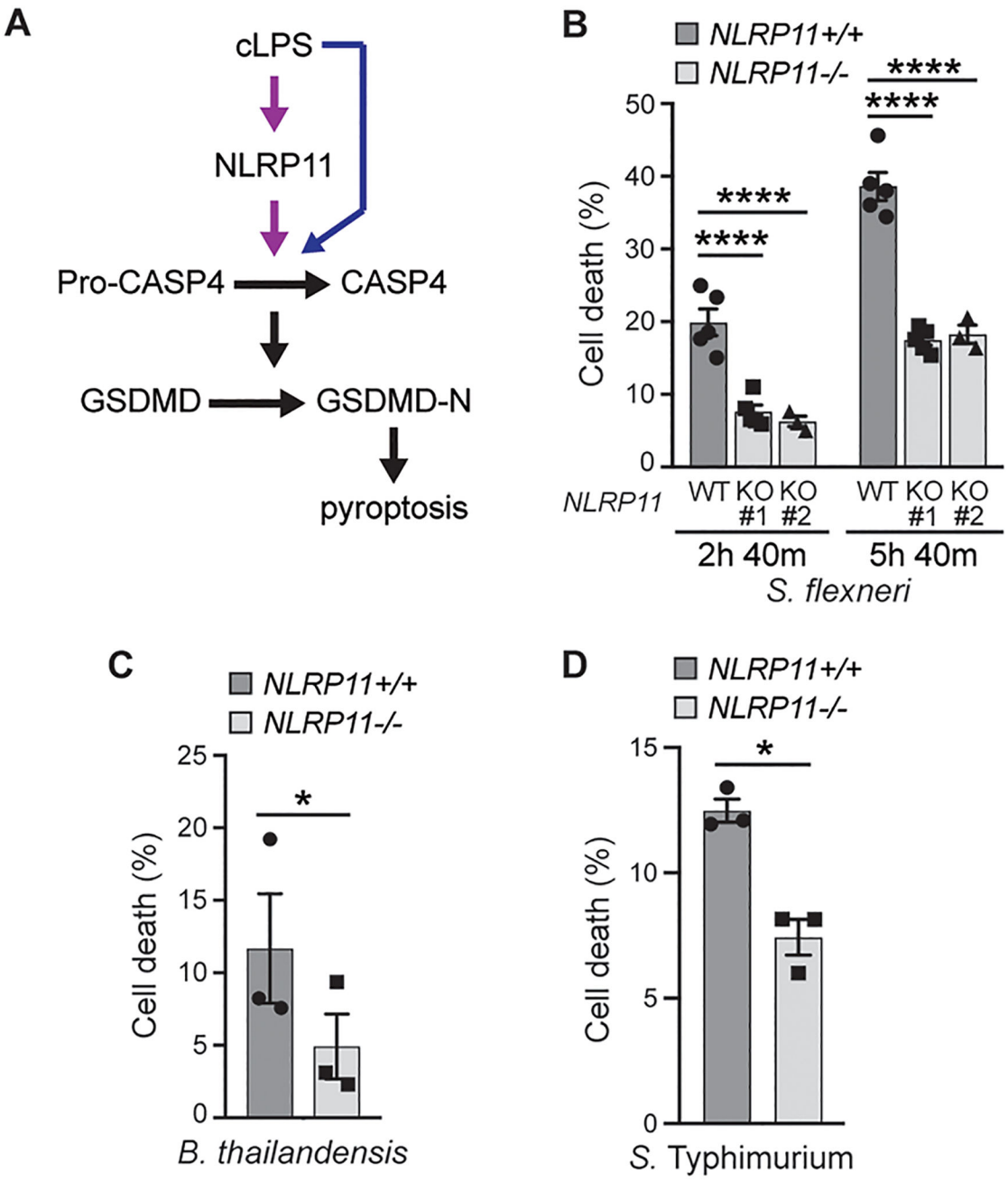

Fig. 1. *NLRP11* is required for efficient cell death induced by infection of human-derived macrophage-like cells with intracellular gram-negative bacteria.

(**A**) Prevailing (blue/black arrows) and proposed (pink/black arrows) paradigms of non-canonical recognition of cLPS, high cLPS concentration activating both pathways. CASP4, caspase-4; GSDMD, gasdermin D; GSDMD-N, GSDMD N-terminal domain. (**B**-**D**) *NLRP11*-dependent death of THP-1 macrophages upon infection with cytosolic *S. flexneri* (**B**) or *B. thailandensis* (**C**), or predominantly vacuolar *S.* Typhimurium (**D**), in two independent (**B**) or one (**C**-**D**) *NLRP11*$^{-/-}$ THP-1 cell lines. $n = 5$ (**B**: WT, KO #1) or 3 biological replicates (**B**: KO #2, **C**-**D**). Cell death, by LDH release, as percent of Triton

X-100 cell lysis. Mean ± S.E.M. Two-way ANOVA with Dunnett *post hoc* test (**B**), or student T-test (**C, D**). *, p<0.05; ***; p<0.001; ****, p<0.0001.

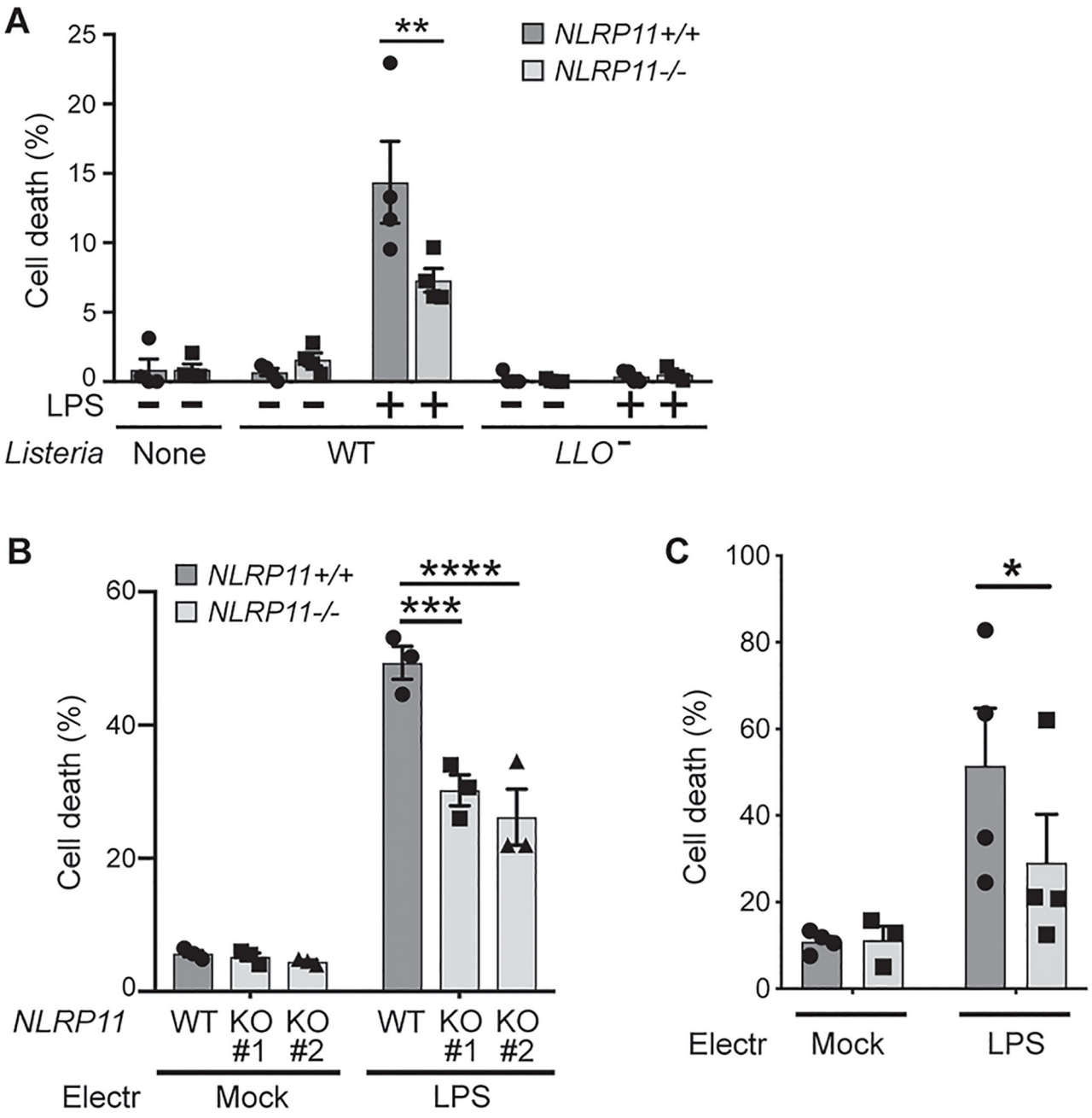

Fig. 2. *NLRP11* potentiates macrophage cell death in response to cytosolic LPS.

(**A**) *NLRP11*-dependent death of THP-1 macrophage-like cells upon infection with cytosolic gram-positive pathogen *L. monocytogenes* coated with *S. enterica* serovar Minnesota LPS. Cell death depends on LPS and vacuolar escape, as *L. monocytogenes LLO*⁻ is restricted to the phagosome. $n = 4$ biological replicates. (**B-C**) In *NLRP11*$^{-/-}$ THP-1 macrophages (**B**) or following NLRP11 siRNA (**C**), cell death in response to electroporated LPS is defective. $n =$ 3 (**B**) or 4 (**C**) biological replicates. Cell death measured as in Fig 1. Electr, electroporation; mock, carrier alone; scRNA, scrambled siRNA. Two-way ANOVA with Šidák *post hoc* test

(**A**) or Tukey *post hoc* test (**B**) or two-way ANOVA with mixed-effects analysis (**C**). Mean ± S.E.M. *, $p<0.05$; **, $p<0.01$; ***; $p<0.001$; ****, $p<0.0001$.

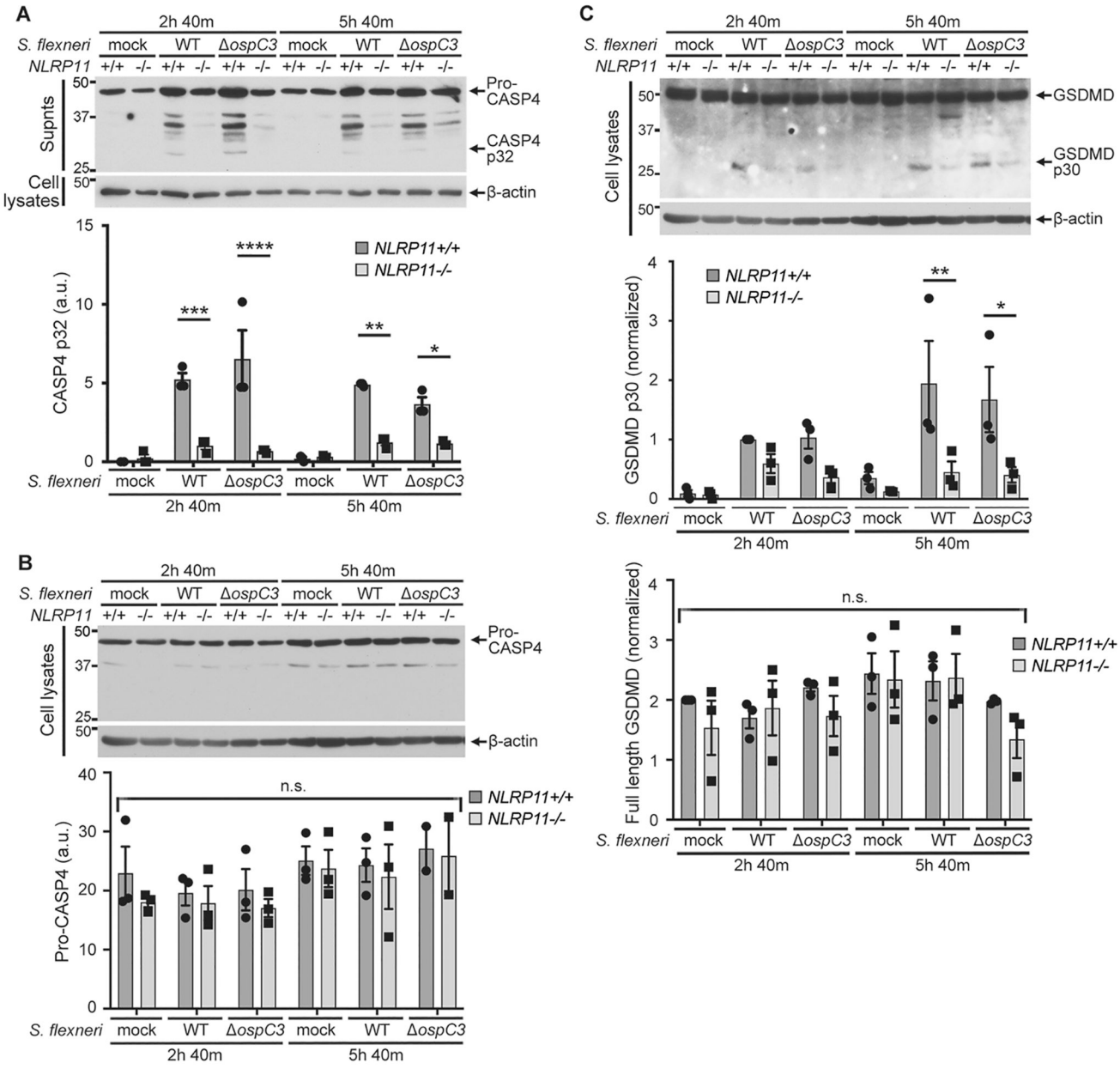

Fig. 3. *NLRP11* is required for processing of caspase-4 and gasdermin D during *S. flexneri* infection.

S. flexneri infection of THP-1 macrophages. (**A**) Processing of caspase-4 (CASP4), with release of p32 polypeptide. Top, representative western blots of culture supernatants (CASP4) and associated cell lysates (β-actin); bottom, corresponding band densitometry of CASP4 p32. (**B**) Levels of pro-CASP4 in cell lysates from experiments described in panel **A**. Top, representative western blots of cell lysates; bottom, corresponding band densitometry of pro-CASP4. (**C**) Processing of gasdermin D (GSDMD), with release of p30 polypeptide. Top, representative western blots of cell lysates; bottom, corresponding band densitometry of GSDMD p30 (top) and full length GSDMD (bottom); in (**C**), densitometry is normalized to band for wildtype (WT) *S. flexneri* infection of NLRP11$^{+/+}$ THP-1

macrophages. In the absence of OspC3, processing of GSDMD was similar to that occurring with WT *S. flexneri* infection (C). $n = 3$ biological replicates. MW markers in kD. Mean ± S.E.M. Two-way ANOVA with Šidák *post hoc* test. *, $p<0.05$; **, $p<0.01$; ***; $p<0.001$; ****, $p<0.0001$; n.s., not significant for any comparison.

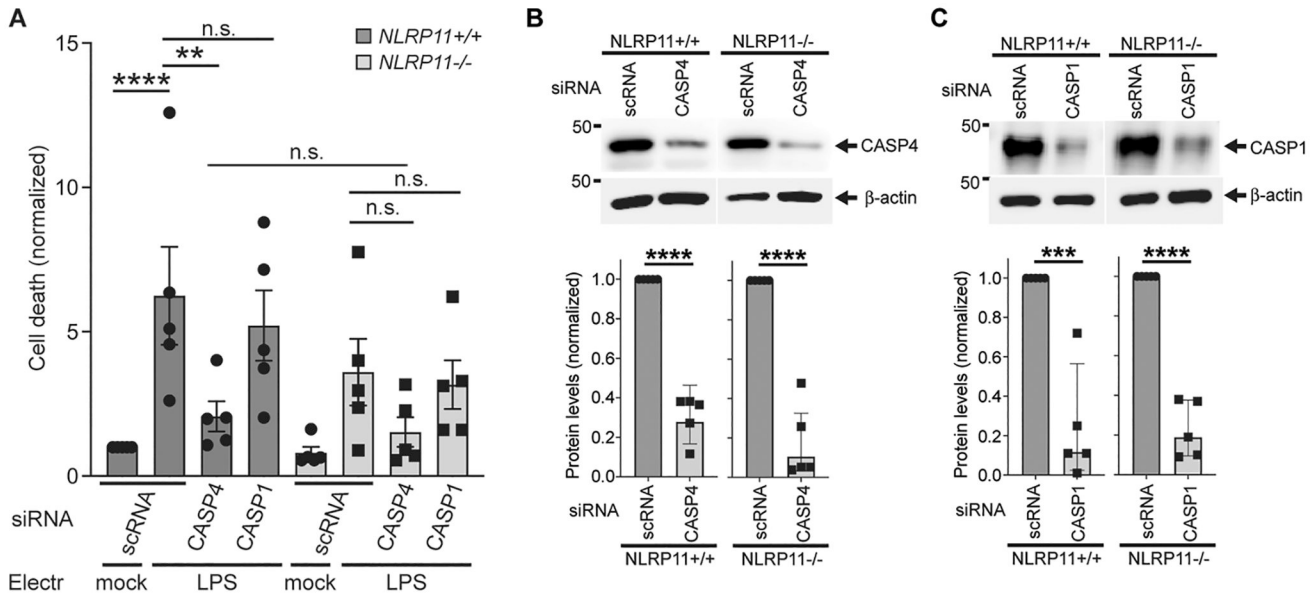

Fig. 4. NLRP11-dependent cell death in response to cLPS is dependent on caspase-4 but independent of caspase-1.

(**A**) Cell death of THP-1 macrophages in response to electroporated LPS following siRNA depletion of *CASP4* or *CASP1*. $n = 5$ biological replicates. Cell death measured as in Fig 1; normalized to mock transfection of *NLRP11*$^{+/+}$ cells following scRNA treatment because data from 5 independent experiments were combined. (**B-C**) Extent of depletion with siRNA of *CASP4* (**B**) or *CASP1* (**C**). $n = 5$ biological replicates. Representative western blots of cell lysates and corresponding band densitometry for each knocked down protein, normalized to protein level in scRNA condition. The western blot panels for each protein within each panel are from the same blot. β-actin, loading control. Electr, electroporation; mock, carrier alone; scRNA, scrambled siRNA; CASP4, caspase-4; CASP1, caspase-1. Two-way ANOVA with Tukey *post hoc* test (**A**) or unpaired student T-test (**B-C**). Mean ± S.E.M. **, p<0.01; ***, p<0.001; ****, p<0.0001; n.s., not significant.

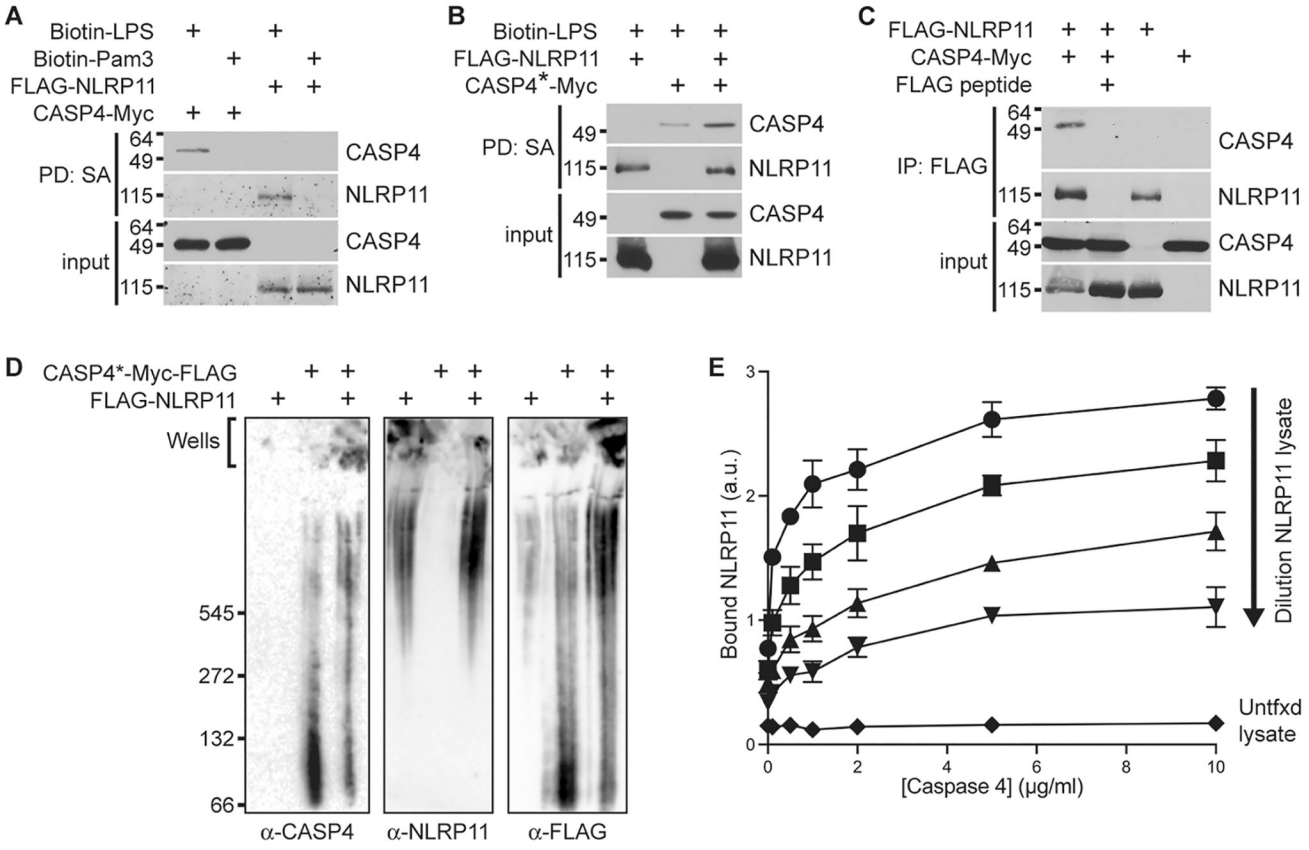

Fig. 5. NLRP11 interactions with LPS and caspase-4

Precipitations from reconstituted HEK293T lysates expressing NLRP11 and/or caspase-4. (**A-B**) Precipitation of NLRP11 and wildtype caspase-4 (CASP4) by biotin-LPS, separately (**A**) and together (**B**), and not biotin-Pam3CSK4 (Pam3) (**A**). PD: SA, precipitation with streptavidin beads. $n = 3$ biological replicates. (**C**) NLRP11 precipitates wildtype CASP4. $n = 3$ biological replicates. (**D**) Shift of CASP4 into higher molecular weights upon co-production with NLRP11. Native gel migration of FLAG-NLRP11 and CASP4-Myc-FLAG; representative western blots of lysates of transfected HEK293T cells. $n = 3$ biological replicates. Native gel MW markers in kD. (**E**) Increasing interaction between NLRP11 and CASP4 as a function of concentration of each protein. FLAG-NLRP11 in transfected HEK293T cells bound to plates coated with purified wildtype CASP4; detection of bound FLAG. NLRP11 lysate dilutions: circles, undiluted; squares, 1:2 dilution; triangles, 1:4 dilution; inverted triangles, 1:8 dilution. Diamonds, untransfected (untfxd) lysate. $n = 3$ biological replicates. a.u., arbitrary units. CASP* (**B** and **D**), catalytically inactive CASP4(C258A).

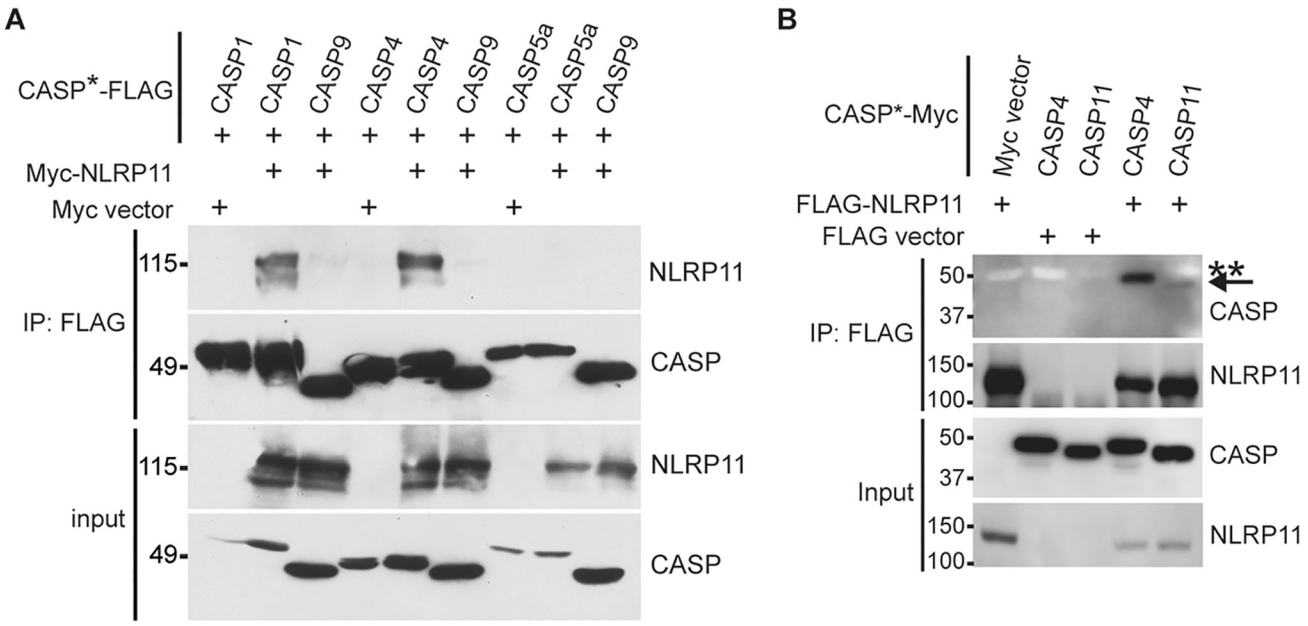

Fig. 6. Specificity of NLRP11 for caspases

Precipitations from reconstituted HEK293T lysates expressing NLRP11 and indicated caspases. (**A**) FLAG-tagged inactive caspase (CASP1[C285A]-FLAG, CASP5a[C315A]-FLAG, CASP9[C287S]-FLAG) precipitation of Myc-NLRP11. (**B**) FLAG-tagged NLRP11 precipitation of inactive mouse caspase-11 (CASP11[C254A]-Myc) versus human caspase-4 (CASP4[C258A]-Myc). Arrow, CASP4 band and weak CASP11 band; **, white band on image, which is non-specific; CASP*, catalytically inactive caspase. IP: FLAG, precipitation with FLAG antibody-coated beads. Representative western blots detection with anti-FLAG or anti-Myc antibody. $n = 3$ experiments (each **A** and **B**). MW markers in kD.

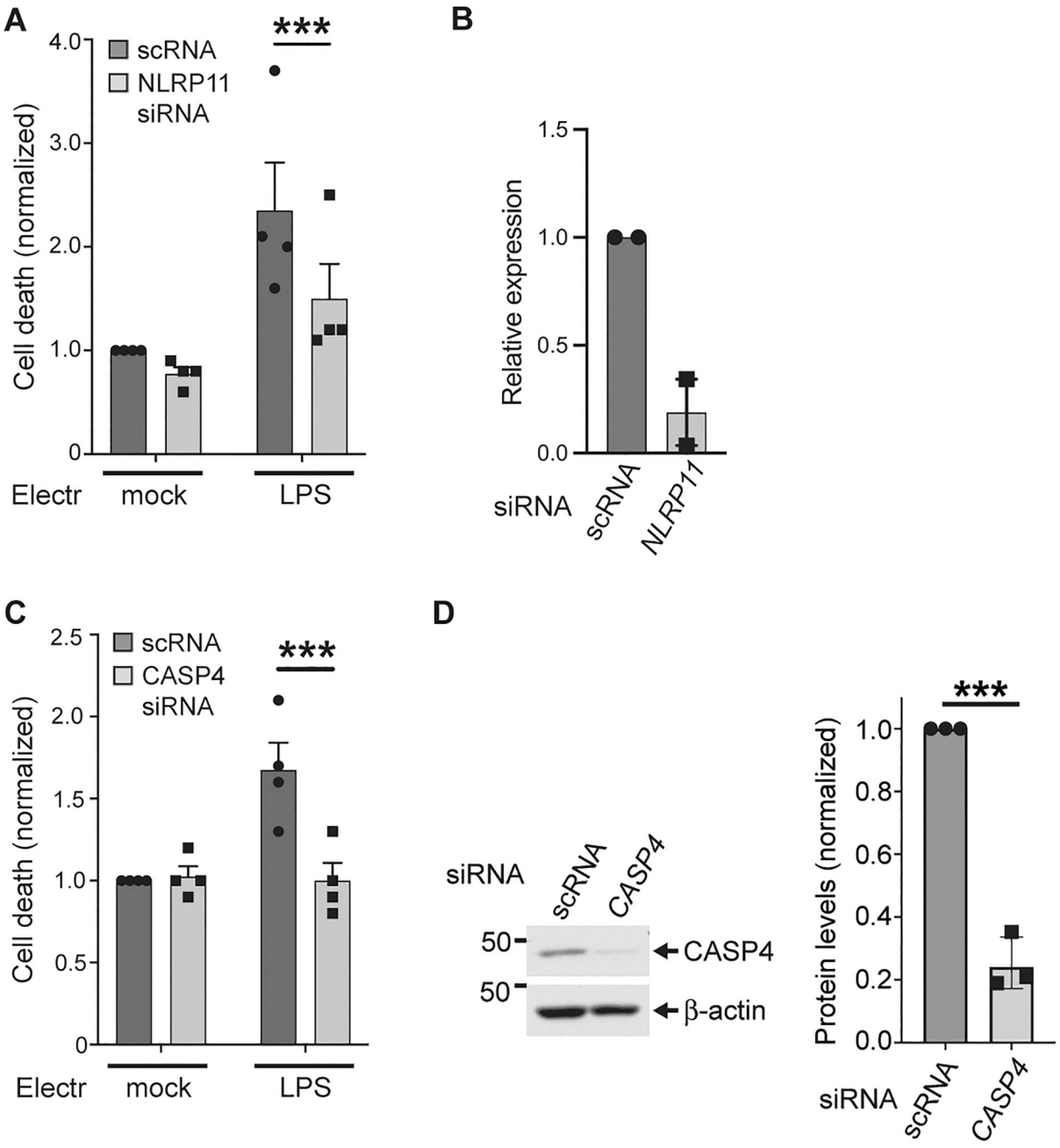

Fig. 7. Requirement for NLRP11 for cell death in response to cLPS in primary human macrophages.

NLRP11-dependent cell death in response to electroporated LPS in isolated primary human monocyte-derived macrophages (CD14+), treated with siRNA to *NLRP11*. (**A**) Cell death in CD14+ macrophages depleted or not for *NLRP11*. (**B**) RT-qPCR analysis of *NLRP11* transcript following siRNA treatment. Representative data from CD14+ cells from a single donor. (**C**) Cell death in CD14+ macrophages depleted or not for *CASP4*. (**D**) Level of caspase-4 (CASP4) depletion. Representative western blots of cell lysates (left) and corresponding band densitometry, normalized to level of protein in scRNA condition (right).

β-actin, loading control. Data are combined from 4 biological replicates (**A** and **C-D**); each replicate was performed with cells from a different individual donor. Cell death measured as in Fig 1; normalized to mock electroporation following scRNA treatment. $n = 4$ experiments. For cell death measurements, an identical number of cells were used for each condition (see Methods). Electr, electroporation; mock, carrier alone; scRNA, scrambled siRNA. Mixed-effects analysis (**A, C**); unpaired student T-test (**D**). Mean ± S.E.M. ***; $p<0.001$.